The International Journal of Advanced Manufacturing Technology (2019) 100:1867–1880
https://doi.org/10.1007/s00170-018-2791-2

ORIGINAL ARTICLE

# Experimental and numerical analysis of grain refinement effect on hot tearing susceptibility for Al–Mg alloys

R. Takai [1,2] · N. Endo [1] · R. Hirohara [1,3] · T. Tsunoda [1,3] · M. Yoshida [1,4]

Received: 26 April 2018 / Accepted: 28 September 2018 / Published online: 10 October 2018


## Abstract

Results of finite element method (FEM) thermal stress analyses during solidification of an Al–Mg alloy with different grain sizes revealed the contribution of the macroscopic strain to the reduction of hot tearing susceptibility by the grain refinement. This study used an elasto-creep model to describe the mechanical behavior of the alloy in the semi-solid state. The grain size–dependence was described using the experimentally determined two parameters of $n$ ($=d\log\dot{\varepsilon}^{c}/d\log\sigma$) and $A$ in the power-law creep model in earlier work. Results showed that grain refinement makes the creep strain distribution more uniform and suppresses the maximum strain value during solidification, which in turn should contribute to reducing the hot tearing susceptibility. This result demonstrates that the grain size–dependence of the two creep parameters during the solidification is a key factor for the quantitative prediction of hot tearing tendency with the consideration of grain size.

**Keywords** Hot tearing · Grain refinement · Al–Mg alloy · Thermal stress analysis · The strain rate sensitivity

## 1 Introduction

Hot tearing, a serious defect, occurs in the casting processes of various alloys. Especially in aluminum alloy, Lees [1] reported that the grain refinement reduces hot tearing susceptibility of an Al–Cu alloy. Lin, Aliravci, and Pekguleryuz [2] and Kimura et al. [3] also reported the same results for Al–Mg and Al–Mn alloys. Therefore, Grandfield, Eskin, and Bainbridge [4] described in their book that the ingot is cast with grain refiner in direct chill (DC) casting. Regarding a mechanism of reducing hot tearing susceptibility by the grain refinement, Pellini [5] and Beshop, Ackerlind, and Pellini [6] presented a theory for the first time, which is now widely accepted. Later on, Campbell [7] presented a quantitative description of the Pellini's theory, i.e., the grain refinement reduces the strain per grain boundary liquid film, which in turn reduces hot tearing susceptibility as written below.

$$\varepsilon_{gb} = \varepsilon_{macro}/N_{gb} \quad (1-1)$$

$$N_{gb} = l/d_g \quad (1-2)$$

$$\varepsilon_{macro} = \alpha\Delta TL/l \quad (1-3)$$

$\varepsilon_{gb}$ and $\varepsilon_{macro}$ are the strain per grain boundary liquid film and the macroscopic strain in the mushy zone respectively. $N_{gb}$ is the number of grain boundary in the mushy zone. $L$ and $l$ are the lengths of the casting and the mushy zone respectively. $d_g$, $\alpha$, and $\Delta T$ are the grain size, the coefficient of thermal expansion, and the temperature decrease from liquids during cooling respectively. Hot tearing can be assumed to occur when $\varepsilon_{gb}$ exceeds a critical value. Regarding the two parameters in the right side of the Eq. (1-1), the number of grain size $N_{gb}$ is obviously a function of the grain size $d_g$. On the other hand, the macroscopic strain $\varepsilon_{macro}$ in Eq. (1-3) is a simple model. Actually, the strain should also be a function of the grain size because the constitutive behavior in the semi-solid state of alloy, which governs the macroscopic strain $\varepsilon_{macro}$, depends on grain size [8], i.e., the grain size must have some non-

✉ R. Takai
rtakai@akane.waseda.jp

[1] Department of Modern Mechanical Engineering, Graduate School of Waseda University, 3-4-1 Shinjyuku-ku Okubo, Tokyo 169-8555, Japan

[2] Present address: IHI Corporation, 3-1-1, Toyosu, Koto-ku, Tokyo 135-8710, Japan

[3] Present address: Honda Motor Co., Ltd., 2-1-1 Minami-Aoyama, Minato-ku, Tokyo 107-8556, Japan

[4] Kagami Memorial Research Institute for Materials Science and Technology, Waseda University, 2-8-26, Nishi-Waseda, Shinjyuku-ku, Tokyo 169-0051, Japan

negligible impact on the macroscopic strain in the mushy zone.

In order to obtain accurate macroscopic strain in the mushy zone of light metal alloy, several reports describing thermal stress analyses have been presented for DC casting and shape casting. Regarding the thermal stress analysis of DC casting during the solidification, Magnin et al. [9] reported that the higher casting speed enhances the hot tearing tendencies of an Al–Cu alloy. Nagaumi and Umeda [10], M'Hamdi et al. [11], and Suytino et al. [12] also reported the same results for Al–Mg–Si and Al–Cu alloys. As to the analysis of shape casting during the solidification, Pokorny et al. [13] reported that the lower mold temperature enhances the hot tearing tendencies of an Mg–Al alloy. Shi et al. [14] reported the effect of both the mold and the pouring temperatures on the hot tearing tendencies of a Ni-base superalloy. In their reports, based on the hot tearing criterion presented by Prokhorov [15], their calculated macroscopic strains were used for the indicator to predict hot tearing tendencies. Despite the above numerous reports, no report in the relevant literature, except for a study reviewed below, has described the incorporation of the grain size–effect when predicting hot tearing.

Using the thermal stress analysis with a constitutive model of an AA5182 alloy in the semi-solid state that Phillion et al. [16] had developed, Jamaly et al. [17] considered the grain size–distribution of the DC casting billet from the center to the surface, which arises from the difference of each cooling rate. In the constitutive model, the strain hardening coefficient depends on the grain size through the liquid film thickness as an intermediate variable. The material parameters including the hardening coefficient are determined from not experimental data but the stress–strain curves obtained through the direct finite element (FE) simulation of semi-solid tensile deformation by Phillion, Cockcroft, and Lee [18]. Therefore, the validity of the analytical result is uncertain.

To clarify the effect of the macroscopic strain on the reduction of hot tearing susceptibility by the grain refinement, thermal stress analyses were conducted during the solidification of an Al–Mg alloy having different grain sizes. An elasto-creep model was used to describe the mechanical behavior of the alloy with the grain size–dependent two creep parameters of $n$ ($=d\log\dot{\varepsilon}^{c}/d\log\sigma$) and $A$ in the semi-solid state. Therein, $\dot{\varepsilon}^{c}$ and $\sigma$ represent the creep strain rate and the flow stress respectively. For the two creep parameters, Takai et al. [19] determined experimentally in earlier work for the coarse grain alloy. Later on, Takai et al. [20] reported the effect of grain refinement on the two parameters. Then, it was examined how the macroscopic strain during the solidification contributes to the reduction of hot tearing susceptibility by the grain refinement. Finally, the reduction of the strain per grain boundary liquid film $\varepsilon_{gb}$ in the Eq. (1-1) by the grain refinement was quantified with the consideration of the grain size–effect on the macroscopic strain $\varepsilon_{macro}$.

## 2 Experimental

### 2.1 Materials

This study used two alloys intended to have two different grain sizes. One is the Japanese Industrial Standard (JIS) AC7A (which corresponds roughly to A514) Al–5 wt.%Mg alloy as a base alloy. The other is the alloy with Ti–B. The base alloy in crucible was heated at furnace. Then, for the alloy with Ti–B, an Al–5Ti–1B master alloy was added to the base alloy after melting. The melting in crucible was stirred immediately before pouring.

Table 1 presents their chemical compositions. Figure 1a presents the relations between the temperature and the solid fraction determined using the Scheil–Gulliver model. Computational thermodynamics software (JMatPro8.0; Sente Software Ltd.) was used for calculations. Consequently, the respective temperatures of the liquidus $T_l$ and solidus $T_s$ were 633 and 448 °C. Before the casting test (described later), the alloys were melted at 800 °C under argon gas atmosphere.

### 2.2 Experimental device

An instrumented casting device [21] was used in order for both quantifying hot tearing susceptibility and measuring the thermal load during solidification under the condition that the contraction was prevented. The two experimental values were used in section III.B to validate both the thermal stress analysis and the prediction of hot tearing susceptibility. Similar devices intended for the same purpose were reported previously for Al–Cu alloys by Stangeland et al. [22] and for Mg–Al alloys by Pokorny et al. [23]. Figure 2a, b presents schematics of both the device and the specimen dimensions used for this study.

In the device, to make the center part of the specimen in the longitudinal direction the final solidification part, two insulating papers were attached on the surface of the stainless steel mold which contacts with the center part of the specimen. In Fig. 2a, one end of the rod with a nut, which is embedded in the specimen after the casting, prevents contraction of the alloy during solidification. Consequently, the final solidification part has the highest potential for hot tearing in the entire specimen.

Figure 2b shows the specimen dimensions. The geometries were determined from the shape of the cavity before casting in the experimental device shown in Fig. 2a. Therefore, the shape of the specimen shown in Fig. 2b has no information about the external shrinkage, which will be described later in Section 2.5.

The specimen temperature at the 10 mm longitudinal offset from the center was measured continuously during testing. The offset eliminates the possibility of crack initiation from the thermocouple at the final solidification part of the

**Table 1** Chemical composition (wt.%) of Al–5 wt.%Mg alloy with and without grain refiner

| Alloy | Cu | Si | Mg | Zn | Fe | Mn | Ni | Ti | B | Al |
|---|---|---|---|---|---|---|---|---|---|---|
| Al–5 wt.%Mg alloy | 0.029 | 0.119 | 4.707 | 0.022 | 0.173 | 0.386 | 0.010 | 0.010 | – | Bal. |
| With grain refiner | 0.030 | 0.088 | 4.693 | 0.022 | 0.169 | 0.381 | 0.010 | 0.063 | 0.009 | Bal. |

specimen. The temperature was defined as the representative value of the specimen temperature.

## 2.3 Cooling rate of the specimen during solidification

Regarding the mechanical behavior of alloys during the solidification, Giraud, Suery, and Coret [24] reported that the tensile strength depends on the cooling rate. Then, Hirohara [25] reported that the material parameters in the power law model also depend on the cooling rate. Therefore, the cooling rate during solidification for the analytical object was made as close as possible to the one for the specimen used to determine the material parameter in the constitutive model.

For the latter, Takai et al. [19, 20] reported that the average cooling rate was 0.46 K/s for the specimen for which the true stress–true strain curve was obtained for the material parameters described in Subsection 3.5.2. For the former, results showed that the specimen cooling rate was 0.46 K/s when the initial mold temperature was 430 °C. Consequently, the initial mold temperature was used for a testing condition. The average cooling rate in this study was determined using Eq. (2).

$$\dot{T} \equiv \frac{T_{\mathrm{l}} - T_{\mathrm{s}}}{t_{\mathrm{T_l}} - t_{\mathrm{T_s}}} \tag{2}$$

Therein, $\dot{T}$ denotes the cooling rate, $T_{\mathrm{l}}$ and $T_{\mathrm{s}}$ are the respective temperatures of the liquidus and the solidus of the alloy shown in Fig. 1. $t_{\mathrm{T_l}}$ and $t_{\mathrm{T_s}}$ respectively stand for the times when the representative temperature of the specimen reaches the liquids and the solidus temperatures. The next section will introduce the experimental procedure used with the testing device.

## 2.4 Experimental procedure

At first, the melting alloy of 720 °C was poured into the cavity after the mold temperature reached the initial value (430 °C). Then the thermal load developing during the solidification was measured continuously. The specimen was detached from the device as the specimen representative temperature reaches to around 350 °C, which is around 100 °C lower than the solidus. Below the temperature, the load was not measured due to the unnecessity for validating the stress analysis result during the solidification. Then the hot tearing susceptibility (*HTS*) and the specimen grain size were measured respectively using the following methods.

To quantify the *HTS* for aluminum alloy, Lin, Aliravci, and Pekguleryuz [2] used the length of cracking for the constrained rod casting test. Kimura et al. [3] also used the length for the I-beam casting cracking test to quantify the *HTS*. Therefore, the *HTS* in this study was quantified experimentally as shown in Fig. 3a using Eq. (3) which was proposed in an earlier report of the literature [3].

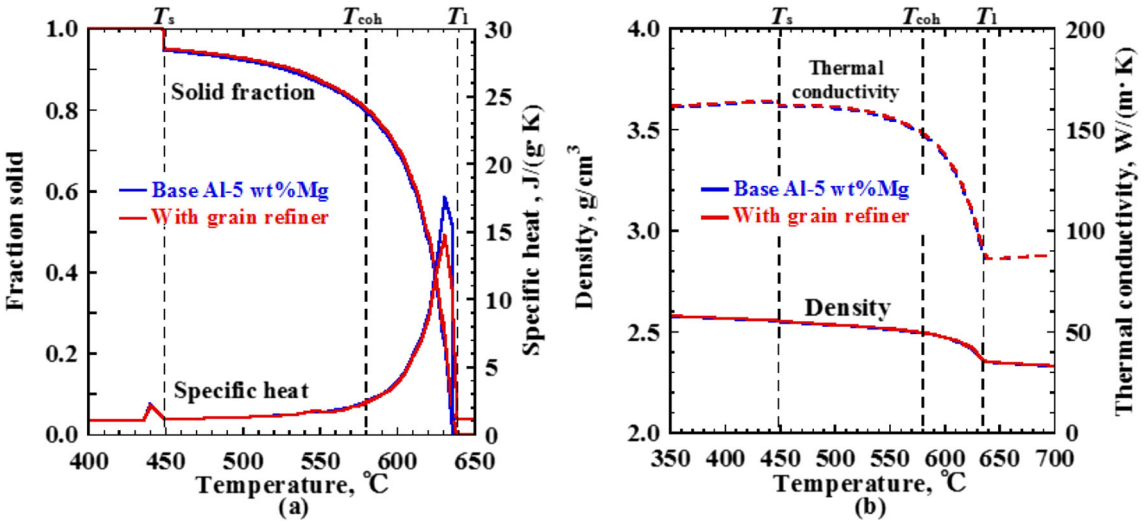


**Fig. 1** Thermophysical properties for Al–5 wt.%Mg alloy without and with grain refiner: **a** solid fraction and specific heat and **b** thermal conductivity and density

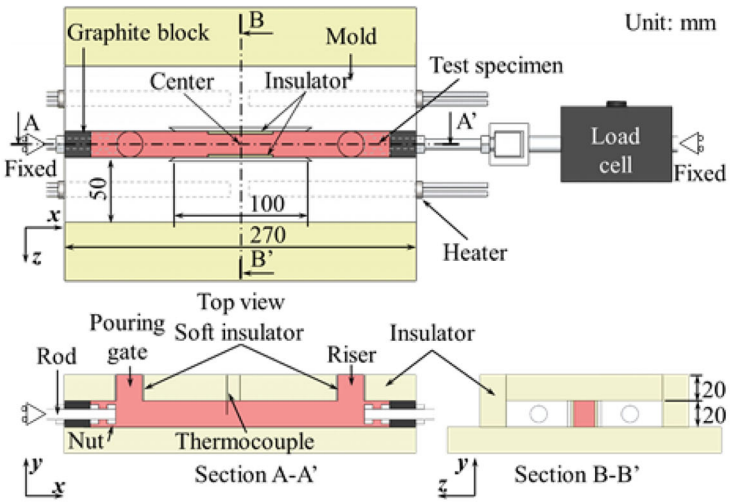


(a)

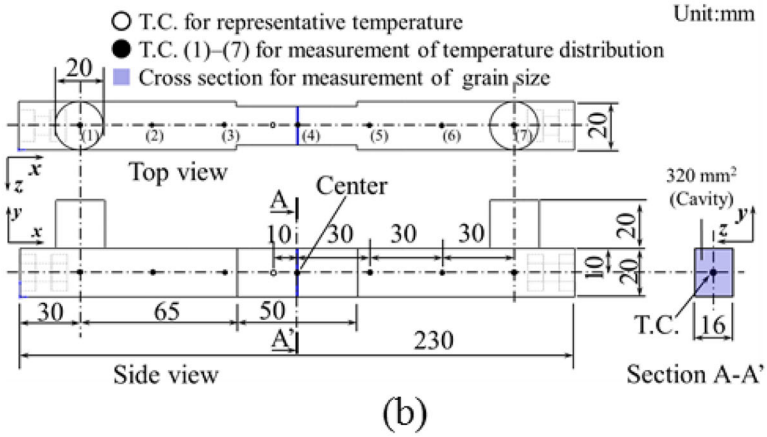


(b)

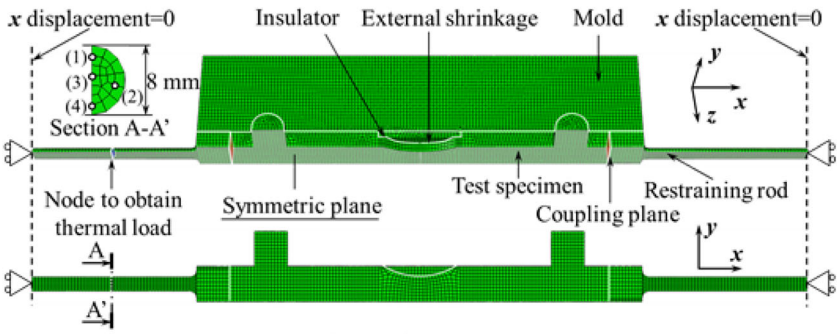


(c)

**Fig. 2** Schematic of instrumented testing device: **a** general view of device, **b** dimension of specimen, and **c** analytical model for thermal stress analysis)

$$HTS \equiv \frac{L_{\text{crack}}}{L_{\text{total}}} \times 100 \tag{3}$$

In the equation, $L_{\text{crack}}$ and $L_{\text{total}}$ respectively represent the crack length and the length of the circumference of the section A-A' at the center part of the specimen marked in Fig. 3a.

The grain size was measured using Eq. (4) at the final solidification part near section A-A'.

$$\overline{d}_{\text{g}} = \sqrt{\frac{4D^2}{N_{\text{g}} \cdot \pi}} \tag{4}$$

Therein, $D^2$ denotes the representative area. $N_{\text{g}}$ represents the number of grains in the area. Here, 6000 μm and 1500 μm were used respectively as the value $D$ for the specimen without and with the grain refiner. The average values of four specimens were obtained for the

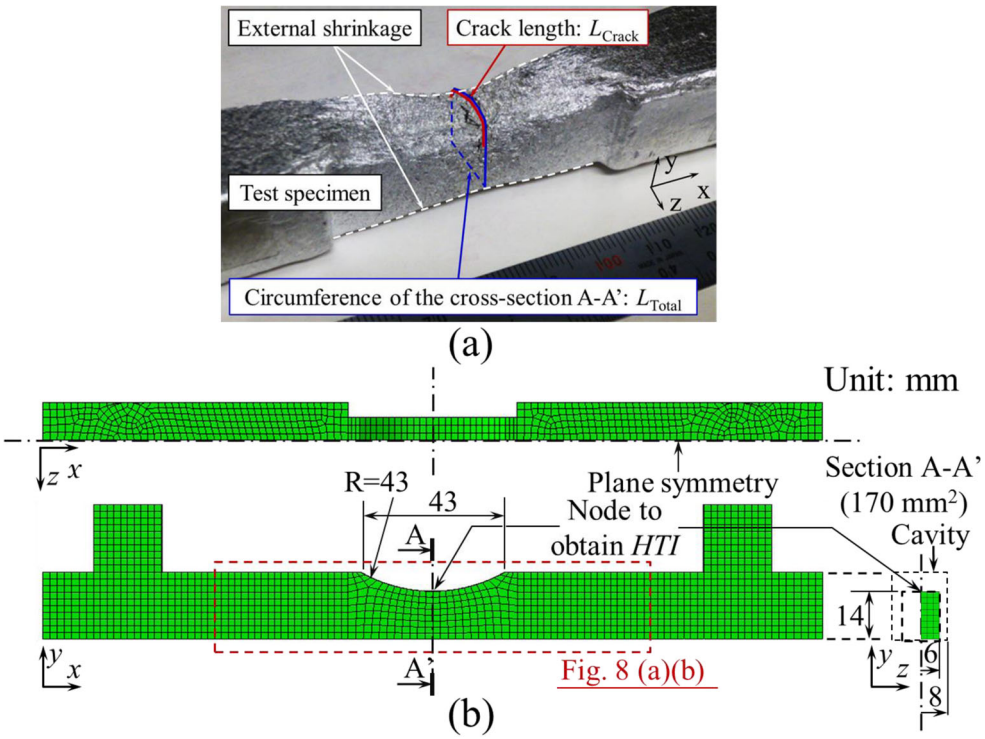


**Fig. 3** **a** Quantification of hot tearing susceptibility using Eq. (3) and **b** analytical model used for the two alloys with the different grain size

representative values of both the HTS and the grain size of each alloy.

### 2.5 Measurement of the cross-sectional area of the specimen at the final solidification part

Figure 3a shows the final solidification part of the specimen after cooling. External shrinkage formed in both $y$ and $z$ directions at the part. Local reduction of the cross-sectional area of the specimen by the shrinkage should influence the strain accumulation during solidification. To reproduce the reduced cross-sectional area in the analytical model of the specimen at the next chapter, the area at section A-A' in Fig. 3a was measured from the specimen after cooling. To measure the area with no cracking, the specimen was solidified with contraction allowed. Based on the measured cross-sectional area, the geometry of the external shrinkage in the analytical model of the specimen was determined in section 3.1.

### 2.6 Measurement of the temperature distribution in the specimen

Before evaluating the validity of the stress analysis during alloy solidification, the temperature distribution of the specimen calculated using thermal analysis must be coincident with the experimentally measured distribution. To validate the thermal analysis result, the temperatures at seven points on the specimen, marked in Fig. 2b, were measured continuously from pouring to the solidification end of the specimen in a preliminary test used for the base alloy shown in Table 1.

## 3 Thermal stress analysis

### 3.1 Analytical models

Both thermal and stress analyses were conducted using the ABAQUS ver.6.14-5 commercial finite element (FE) package. Figure 2c shows a schematic of the analytical models. In the models, the element type was first-order hexahedral with 2-mm mesh size.

Both the graphite block and the rod on the both ends of the specimen were combined into a single part. Then, the part was newly defined as the "restraining rod". The boundary condition to prevent contraction of the specimen in the stress analysis is described in Section 3.3.

As explained in Section 2.5, external shrinkage was observed at the final solidification part of the specimen. Table 2 presents the measured cross-sectional area A-A' of the specimen at the shrinkage marked in Fig. 3a for the two alloys. The area with the shrinkage was 170–180 mm$^2$, which is around 60% of the area in the cavity (320 mm$^2$). The solver used for this study does not provide solidification analysis that can simulate external shrinkage. For that reason, an analytical model having an external shrinkage was prepared for the thermal stress analyses. Figure 3b depicts the geometry of the analytical model. The cross-sectional area at the shrinkage

**Table 2** Experimental results of grain size, hot tearing susceptibility, and cross-sectional area of the specimen with external shrinkage

| | Grain size*, μm | *HTS** quantified using Eq. (3) | Area of the section* A-A' in Fig. 3a, $mm^2$ |
|---|---|---|---|
| Al–5 wt.%Mg alloy | 600 ± 60 | 32.2 ± 9 | 171 ± 8 |
| With grain refiner | 130 ± 10 | 0 | 181 ± 3 |

*All the data are average values of four samples

was determined to be 180 $mm^2$. Then the same model was used for the two alloys with the different grain sizes in the analyses.

To examine how the existence of the external shrinkage influences on the strain distribution, further thermal stress analysis was conducted using the analytical model of the specimen with no shrinkage. Then, the analytical result will be compared with the result using the analytical model with the shrinkage.

### 3.2 Thermal analysis

The thermophysical properties for each analytical model were determined using the computational thermodynamics software (JMatPro8.0; Sente Software Ltd.). Figure 1 shows the properties of the Al–5 wt.%Mg alloys without and with the grain refiner. Except for around10% reduction in the specific heat at the temperature below the liquids, the grain refiner has negligible impacts on the properties. Besides, to disclose how the grain refinement influences the calculated strain distribution through the material parameters in the constitutive model, it is favorable to use the same result of thermal analysis for the two alloys with the different grain sizes. From the above two reasons, the thermophysical properties of the alloy without the grain refiner are only used for the thermal analysis. Then, using the same thermal analytical result, the stress analyses were conducted for the two alloys without and with the grain refiner.

The initial temperatures of both the specimen and the mold were set at 720 °C and 430 °C in accordance with the experimental conditions.

Figure 4a shows the temperature histories of the specimen for both experimental and analytical results. The stress analysis was conducted using the above thermal analytical result. Based on the experimentally obtained temperature distribution shown in Fig. 4b, the thermal analysis was conducted under the condition that the distribution of the specimen was symmetric in the $x$ direction with respect to the center.

### 3.3 Stress analysis

As shown in Fig. 2c, the two boundary conditions were given to simulate the experimental condition for which the specimen contraction during solidification was prevented. Firstly, the displacement of the end of the restraining rod was fixed in the $x$ direction. Secondly, the nodes on the planes of both the rod and the specimen were coupled where they contact.

The calculated values of both the thermal load and a hot tearing indicator (*HTI*) were obtained from the stress analysis result using the following methods respectively.

Firstly, the load value was obtained using Eq. (5).

$$F_{\text{calculated}} \equiv \frac{\sigma_{xx,1} + \sigma_{xx,2} + \sigma_{xx,3} + \sigma_{xx,4}}{4} \times A_{\text{rod}} \tag{5}$$

In that equation, $F_{\text{calculated}}$ represents the calculated value of the thermal load. $\sigma_{xx,1}$, $\sigma_{xx,2}$, $\sigma_{xx,3}$, and $\sigma_{xx,4}$ are the respective predicted values of the stresses in the $x$ direction at the four nodes of the rod marked in Fig. 2c. $A_{\text{rod}}$ is the cross-sectional area of the rod.

Secondly, the *HTI* was defined as follows in this study using the macroscopic strain in the mushy zone based on the hot tearing models and/or the criterion that Prokhorov [15] presented.

$$\left.\begin{array}{l} HTI \equiv \varepsilon_1^{\mathrm{c}}(T) - \varepsilon_1^{\mathrm{c}}(T_{\text{coh}}) \\ T_{\text{coh}} \geq T \geq T_{\text{s}} \end{array}\right\} \tag{6}$$

Therein, $\varepsilon_1^{\mathrm{c}}(T)$ represents the maximum principal strain of the creep component at any temperature in the range between the mechanical coherency $T_{\text{coh}}$ and the solidus $T_{\text{s}}$. $T$ is the temperature and $\varepsilon_1^{\mathrm{c}}(T_{\text{coh}})$ is the maximum principal strain of the creep component at the temperature of the mechanical coherency. Especially in aluminum alloy, Singer and Cottrell [26] and Dahle and Aenberg [27] reported that the critical temperature for the occurrence of hot tearing is in the range between mechanical coherency $T_{\text{coh}}$ and solidus $T_{\text{s}}$. Therefore, the *HTI* was defined as the accumulated maximum principal strain of the creep component $\varepsilon_1^{\mathrm{c}}$ at the temperature range. The temperature of mechanical coherency (570 °C (Takai et al. [19, 20]) and solidus $T_{\text{s}}$ of the alloys are shown in Fig. 1. Earlier works [8, 27–29] show that the grain refinement lowers the mechanical coherency temperature where the strength starts to arise in the semi-solid state of alloys during the solidification. This result indicates that the dendrite coherency occurs at a higher solid fraction in the grain-refined structure than in the coarse dendritic structure [27–29]. However, for this Al–Mg alloy, an earlier work [20] shows experimentally that the coherency temperature is around 570 °C regardless of grain size. Through the Eq. (6), the relative difference of the hot tearing susceptibility was predicted for the two alloys.

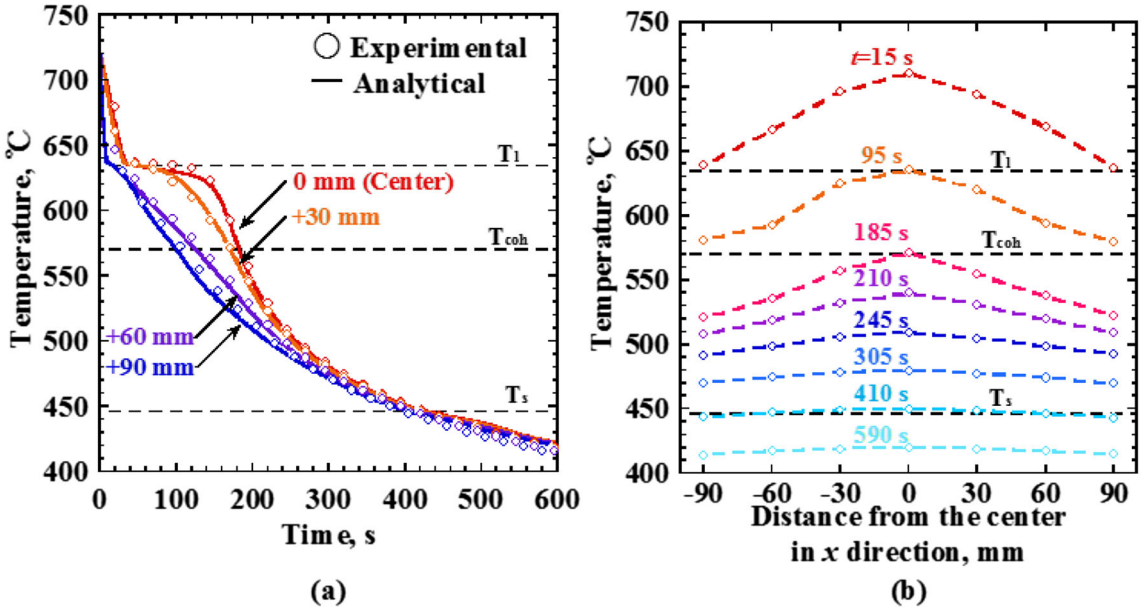


**Fig. 4** Temperature history of the specimen during the solidification: **a** comparison of the cooling curves produced from experimentally obtained result and the analytical one and **b** experimental result of the temperature distribution in the specimen

### 3.4 Constitutive models for the two Al–5 wt.%Mg alloys

The mechanical behavior was described using a thermo-elasto-creep model for temperatures from the liquid state to the solid state including the semi-solid state.

$$\varepsilon^{\text{total}} = \varepsilon^{\text{th}} + \varepsilon^{\text{e}} + \varepsilon^{\text{c}} \tag{7}$$

$$\varepsilon_{ij}^{\text{th}} = \alpha(T)(T - T_{\text{ref}})\delta_{ij} \tag{8}$$

$$\sigma_{ij} = D_{ijkl}\varepsilon_{kl}^{\text{e}} \tag{9}$$

$$D_{ijkl} = f(E(T), \nu(T)) \tag{10}$$

$$\dot{\varepsilon}_{ij}^{\text{c}} = \frac{3\dot{\bar{\varepsilon}}^{\text{c}}}{2\bar{\sigma}}\sigma_{ij}' = \frac{3}{2}A(T)\bar{\sigma}^{n(T)-1}\sigma_{ij}' \tag{11}$$

$$\dot{\bar{\varepsilon}}^{\text{c}} = A(T)\bar{\sigma}^{n(T)} \tag{12}$$

Here, $\varepsilon^{\text{total}}$, $\varepsilon^{\text{th}}$, $\varepsilon^{\text{e}}$, and $\varepsilon^{\text{c}}$ signify the total strain, the thermal strain, the elastic strain, and the creep strain respectively. $\varepsilon_{ij}^{\text{th}}$ is the thermal strain tensor, $\alpha(T)$ is the average linear expansion coefficient, and $\delta_{ij}$ signifies Kronecker delta. $T_{\text{ref}}$ stands for the reference temperature: 570 °C was used for this study. $\sigma_{ij}$ and $\varepsilon_{kl}^{\text{e}}$ denote the stress and the elastic strain tensor respectively. $D_{ijkl}$ represents the elasticity tensor as a function of the Young's s modulus $E$ ($T$) and the elastic Poisson's ratio $\nu$ ($T$) respectively. $\dot{\varepsilon}_{ij}^{\text{c}}$ is the creep strain rate tensor. $\dot{\varepsilon}_{ij}^{\text{c}}$ is derived from the creep potential which is a function of the von Mises stress $\bar{\sigma}$ presented by Odqvist [31]. Therefore, the relation between the equivalent creep strain rate and the von Mises stress is described as the Norton–Bailey law [32, 33] shown in the Eq. (12). In the stress analysis of this study, the plastic strain $\varepsilon^{\text{p}}$ was neglected for the reason explained below. Regarding the constitutive behavior of an Al–Mg alloy at high temperature, Alankar and Wells [30] reported that the alloy at the temperature above 623 K (350 °C) shows no strain hardening behavior. However, as the result of the temperature fields of the specimen shown in Fig. 4b, the temperatures at the edge of the specimen (90 mm from the center) were higher than 430 °C when the final solidification part ends the solidification. Therefore, neglecting the plastic strain contributing to strain hardening should have no effect on the analytical result during the solidification.

The temperature dependences of the material parameters in the constitutive models were summarized in Fig. 5. Their determining methods were shown in Table 3 and the detail will be described in the next section.

### 3.5 Determination of material parameters of the constitutive model for the Al–5 wt.%Mg alloy

#### 3.5.1 Temperature range between the room temperature (25 °C) and just below the solidus (447 °C)

The Young's modulus, the elastic Poisson's ratio, and the average expansion coefficient shown in Fig. 5a, b were obtained from the computational thermodynamics software using the chemical compositions of the Al–5 wt.%Mg alloy without the grain refiner listed in Table 1. For both the two creep parameters of both $n$ ($T$) and $A$ ($T$) shown in Fig. 5c, d, the experimental values [30] of an AA5182 Al–5 wt.%Mg alloy were used in the temperature range from 350 °C to 447 °C.

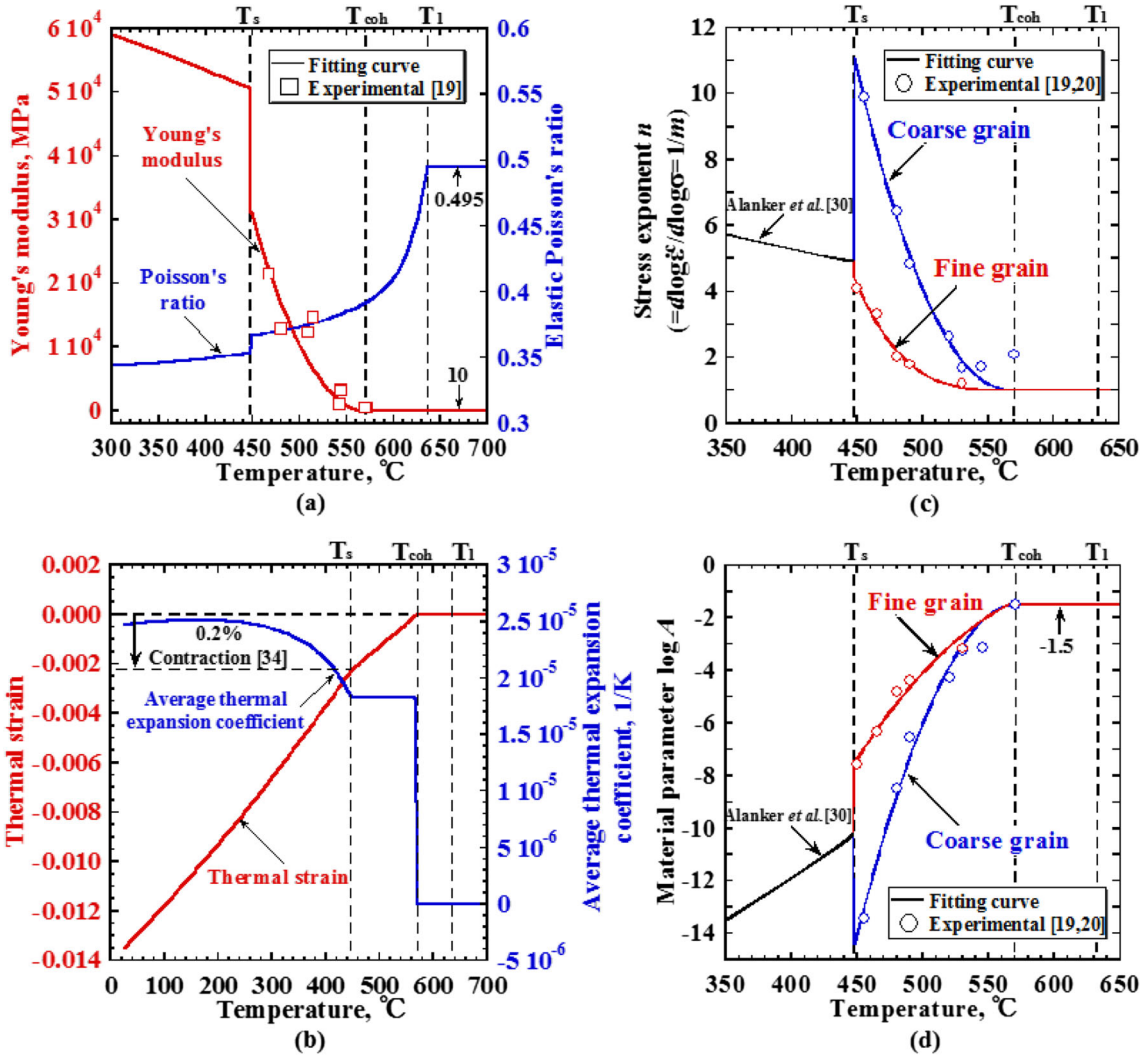


**Fig. 5** Material parameters of thermo-elasto-creep constitutive model for Al–5 wt.%Mg alloy **a** elastic, **b** thermal contraction, and (**c**, **d**) creep parameters

### 3.5.2 Temperature range between the solidus (448 °C) and the mechanical coherency (570 °C)

The plots for both the Young's modulus and the two creep parameters shown in Fig. 5a, c, d were obtained previously using a tensile testing device during solidification [19, 20]. The elastic Poisson's ratio was determined from the computational thermodynamics software. The thermal strain shown in Fig. 5b was determined from the experimental result reported by Eskin et al. [34] that an Al–4 wt.%Mg alloy contracts by around 0.2% from the coherency temperature 570 °C to the solidus. The average expansion coefficient was derived by substituting the thermal strain $\varepsilon^{th}$ into the Eq. (8). For Al–Mg alloy, the grain size–dependence of the contraction during

**Table 3** Determination method of the material parameters of the constitutive model for Al–5 wt.%Mg alloy

| Temperature range, °C<br>Solid fraction $f_s$ | $720 \geq T \geq 633$ ($T_l$)<br>$f_s = 0$ | $633 > T > 570$ ($T_{coh}$)<br>$0 < f_s < 0.85$ | $570$ ($T_{coh}$) $\geq T \geq 448$ ($T_s$)<br>$0.85 \leq f_s \leq 1$ | $447 > T \geq 350$<br>$f_s = 1$ | Figure |
|---|---|---|---|---|---|
| Young's modulus $E$ ($T$) | 10 MPa [17] | 10 MPa [17] | Unloading test for alloy with grain size of around 600 μm [19] | Calculated* | Fig. 5a |
| Elastic Poisson's ratio $n$ ($T$) | 0.495 | Calculated* | Calculated* | Calculated* | |
| Creep parameter $n$ ($T$) | 1 (assumed to be a Newtonian fluid) | | Tensile test for two grain size [19, 20] | Compression test [30] | Fig. 5c |
| Creep parameter $A$ ($T$) | $A$ ($T$) ≡ $A$(570 °C) | | | | Fig. 5d |
| Thermal strain $\varepsilon^{th}$ ($T$) | $\varepsilon^{th}$ ($T$) = $\varepsilon^{th}$ (570 °C) | | Contraction measurement [34] | Calculated* | Fig. 5b |

*Value calculated from a computational thermodynamics software using chemical composition of base alloy in Table 1

the solidification has never been clarified, in contrast to the other aluminum alloys reported by Stangeland et al. [35]. Therefore, for the stress analysis, the grain size–dependence of the thermal strain was neglected.

The two creep parameters of both $n$ ($T$) and $A$ ($T$) were also referred from reports of earlier studies [19, 20], which conducted tensile tests with various tensile speeds for the alloy with the different grain sizes of around 600 and 100 μm at each solid fraction. Regarding the stress exponent $n$ ($T$) for the coarse grain one, the maximum value of around 10 is significantly higher compared to the value at the temperature below the solidus [30]. Such the high values in the semi-solid state were also reported for AA1201 and AA3104 by Drezet and Eggeler [36] and for AA6060 by Giraud et al. [24]. However, nothing has been explained for these values.

#### 3.5.3 Temperature range between the mechanical coherency (570 °C) and the initial temperature of the analysis (720 °C)

The temperatures above mechanical coherency are out of the critical temperature range for the occurrence of hot tearing in aluminum alloy. Therefore, for the stress analysis intended for hot tearing prediction, the material parameters at the temperatures above the mechanical coherency are less important than those at the temperatures below the mechanical coherency. Using the parameters presented below, viscus flow behavior of the alloy was expressed in the temperature range higher than the mechanical coherency.

For the Young's modulus shown in Fig. 5a, the value of 10 MPa assumed by Jamaly, Phillion, and Drezet [17] was used, which is sufficiently smaller compared to the value of the alloy in the solid state.

For the elastic Poisson's ratio shown in Fig. 5a, the value was obtained from the computational thermodynamics software using the chemical compositions of the Al–5 wt.%Mg alloy without the grain refiner listed in Table 1.

For the two creep properties shown in Fig. 5c and d, the values at temperatures above mechanical coherency (570 °C) were determined as follows.

$$n(T \geq T_{\mathrm{coh}}) \equiv 1 \tag{13}$$

$$A(T \geq T_{\mathrm{coh}}) \equiv A(T_{\mathrm{coh}}) \tag{14}$$

Firstly, the stress exponent $n$ ($T$) was determined to be 1 under the assumption that the alloy behaves as a Newtonian fluid. Secondly, the creep parameter $A$ ($T$) was determined to be the value at the mechanical coherency (570 °C) described in the previous subsection because of the difficulty in experimental determination.

The average expansion coefficient was determined as follows. In the temperature range above mechanical coherency, there should be liquid channel network. In such a structure, Stangeland et al. [35] and Hao et al. [37] regarded that the solidification shrinkage should be compensated by liquid feeding. Therefore, the thermal strain in the temperature range was defined to be constant and equal to the value at the mechanical coherency (570 °C). The average expansion coefficient was determined from the thermal strain.

### 3.6 Constitutive models for the restraining rod and the material parameters

The analytical model of the rod was described as an isotropic elastic body. The temperature dependences of the Young's modulus and the elastic Poisson's ratio were determined using the computational thermodynamics software. Their temperature dependence was described by the following functions.

$$E(T) = 1.9868 \cdot 10^{5} - 6.5166 \cdot 10^{1} T - 1.763 \cdot 10^{-2} T^{2} \quad (\text{Unit : MPa}) \tag{15}$$

$$\nu(T) = 2.9525 \cdot 10^{-1} + 4.4077 \cdot 10^{-5} T + 2.0833 \cdot 10^{-11} T^{2} \tag{16}$$

Since it was confirmed that the thermal expansion of the rod has negligible impact on the analytical result, the thermal expansion was neglected in this study.

## 4 Results and discussions

### 4.1 Experimental results

This section presents experimentally obtained results of the thermal load and the hot tearing susceptibility (*HTS*) for comparison with their corresponding calculated values.

Firstly, Table 2 shows both *HTS* quantified using Eq. (3) and the grain sizes obtained using Eq. (4). Figure 6 shows that the grain morphology changed from coarse dendritic to fine equiaxed dendritic through refinement. Hot tearing was observed in the base alloy with coarse grain ($\overline{d}_{\mathrm{g}} = 600$ μm), but no visible crack was observed in the fine grain alloy ($\overline{d}_{\mathrm{g}} = 130$ μm).

Secondly, Fig. 7a, b presents experimentally obtained thermal loads that develop during solidification. In Section 4.2, the above two experimental results will be used to validate the calculated values of the thermal load and the hot tearing indicator (*HTI*).

### 4.2 Evaluation of the validity in the analytical values of both the thermal load and the *HTI*

#### 4.2.1 Comparison of the thermal loads between the calculated value and experimental one

Figure 7a, b presents a comparison of the accumulated thermal load during solidification between the calculated value and the

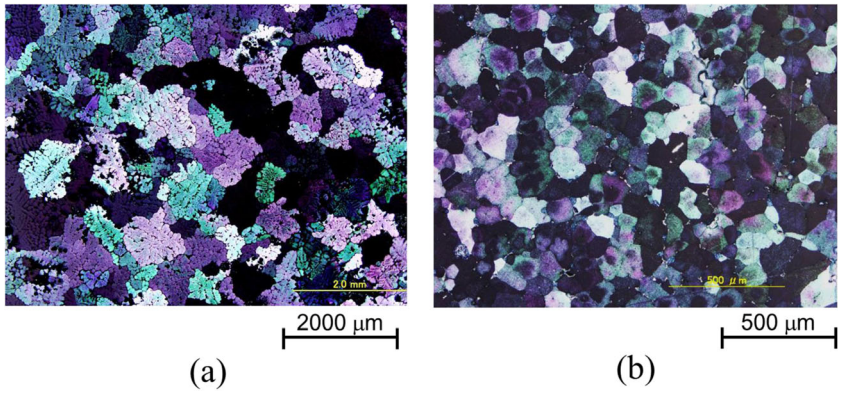


**Fig. 6** Grain morphologies of the test specimen obtained at the surface of section "A-A" marked in Fig. 2b: **a** coarse equiaxial dendritic and **b** fine equiaxial dendritic structures

experimental one for alloys of the two grain sizes. The calculated results were obtained using the analytical model with the external shrinkage described in Section 3.1.

Regarding the thermal load at the temperature of solidus for the coarse grain alloy, the calculated value was two times higher than the experimental one. The difference between the two values is expected to arise because of the following reason. The experimental value was derived when the initiation of the crack and the propagation released the load in the coarse grain alloy. However, the analytical value did not reflect the cracking behavior described above. For the grain-refined alloy, the calculated value of the thermal load at the temperature of the solidus was around 80% of the experimental value. No visible crack in the specimen for the grain-refined alloy can produce a better agreement between the two values than that of the coarse grain alloy. Based on the results described above, the calculated value of the thermal load showed good agreement with the experimentally obtained value in the conditions that include no hot tearing.

#### 4.2.2 Comparison between the calculated value of the *HTI* and the experimentally quantified value of *HTS*

Figure 8a, b shows the contours of the maximum principal strain of the creep component at the surface marked in Fig. 3b when the specimen had solidified completely. The location where the strain is maximum in the analytical model is consistent with the location in the specimen where hot tearing was observed for the coarse grain alloy, as shown in Fig. 3a. Therefore, using Eq. (6), *HTI* was obtained at the node where the strain shows the maximum.

Figure 7c presents the calculated value of the accumulation of the *HTI*s during the solidification for alloys with the different grain sizes. The value of the grain-refined alloy was around 35% smaller than that in the coarse grain alloy. The *HTI* in the Eq. (6) can be regarded as the more accurate macroscopic strain rather than the Eq. (1-3). In order to evaluate the reduction factor of the strain $\varepsilon_{gb}$ (the strain per grain boundary liquid film) by the grain refinement with the consideration of the effect of the

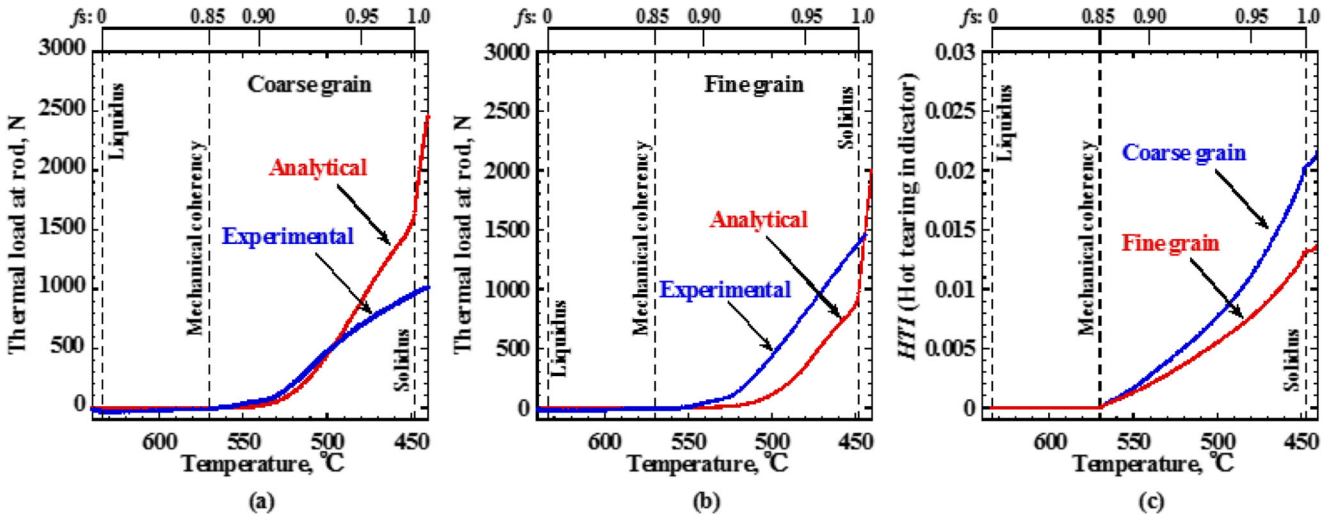


**Fig. 7** Analytical results of thermal stress analyses using specimen model with external shrinkage: thermal loads obtained using Eq. (5) with the experimental ones (**a**, **b**) and hot tearing indicators (*HTI*s) obtained using Eq. (6) for coarse grain alloy and fine grain alloy (**c**)

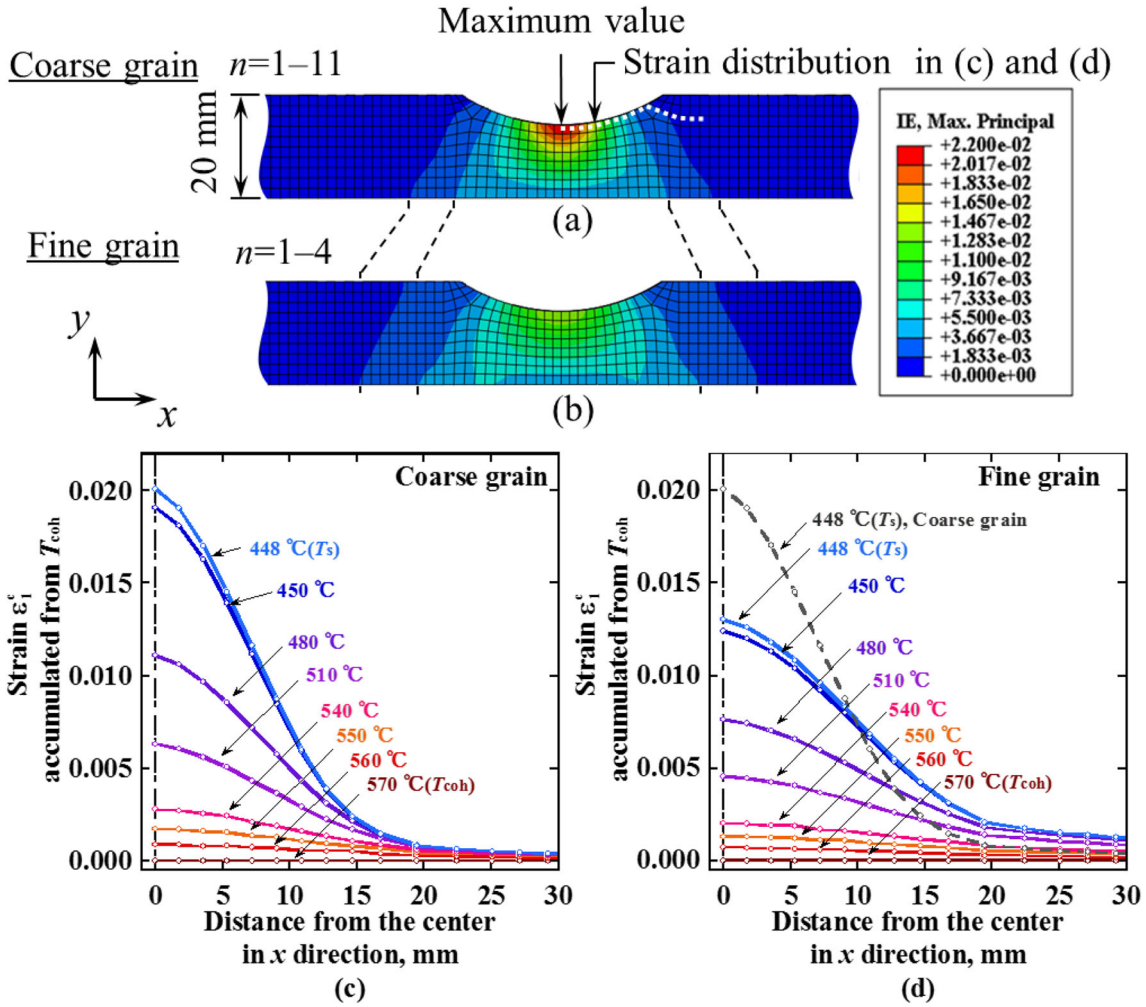


**Fig. 8** Both contour plot and distribution of the maximum strain of the creep component: coarse grain (**a**, **c**) and fine grain (**b**, **d**)

macroscopic strain, following description is derived from the Eq. (1-1).

$$\frac{\varepsilon_{gb}{}^{CG}}{\varepsilon_{gb}{}^{FG}} = \frac{\varepsilon_{macro}{}^{CG}}{\varepsilon_{macro}{}^{FG}} \frac{N_{gb}{}^{FG}}{N_{gb}{}^{CG}} \left( = \frac{\varepsilon_{macro}{}^{CG}}{\varepsilon_{macro}{}^{FG}} \frac{d_g{}^{CG}}{d_g{}^{FG}} \frac{l^{FG}}{l^{CG}} \right) \tag{17}$$

The superscripts of "CG" and "FG" mean coarse grain and fine grain respectively. The reduction factor of $\varepsilon_{gb}$ is composed of the two factors. The one is $\varepsilon_{macro}{}^{CG}/\varepsilon_{macro}{}^{FG}$ and the value is 1.53 (=0.0201/0.0131) from the results of FEM thermal stress analysis. The other is $N_{gb}{}^{FG}/N_{gb}{}^{CR}$ and the value is 4.62 (=600/130) under the assumption that $l^{CG}/l^{FG} = 1$, i.e., the length of hot spot is independent of the grain size. Therefore, the total reducing factor $\varepsilon_{gb}{}^{CG}/\varepsilon_{gb}{}^{FG}$ is calculated to be 7.08 (=4.62 × 1.53), which shows 86% (=1 − 1/7.08) reduction of the strain $\varepsilon_{gb}$ by the grain refinement. The quantitative estimation should be consistent with the experimentally quantified *HTS* shown in Table 2. In the next section, the reason for the smaller value of the *HTI* in the grain-refined alloy compared to the coarse grain alloy will be discussed.

## 4.3 Strain distribution around the final solidification part of the specimen during solidification

### 4.3.1 Specimen with external shrinkage

Figure 8c, d presents the distributions of the maximum principal strain of the creep component $\varepsilon_1^c$ accumulated from the mechanical coherency along the white broken line marked in Fig. 8a, b for the two alloys with different grain sizes. Comparison of the macroscopic strain distribution between the two grain sizes revealed that the grain refinement makes the strain distribution more uniform and suppresses the maximum value of the strain, which in turn can be expected to contribute to reducing the susceptibility to hot tearing. Above result is consistent with an earlier work reported by D'Elia, Ravindran, and Sediako [38] who carried out neutron diffraction strain mapping on the casting after cooling. The report shows that the grain refinement makes the residual strain distribution uniform and contributes to higher resistance to hot tearing.

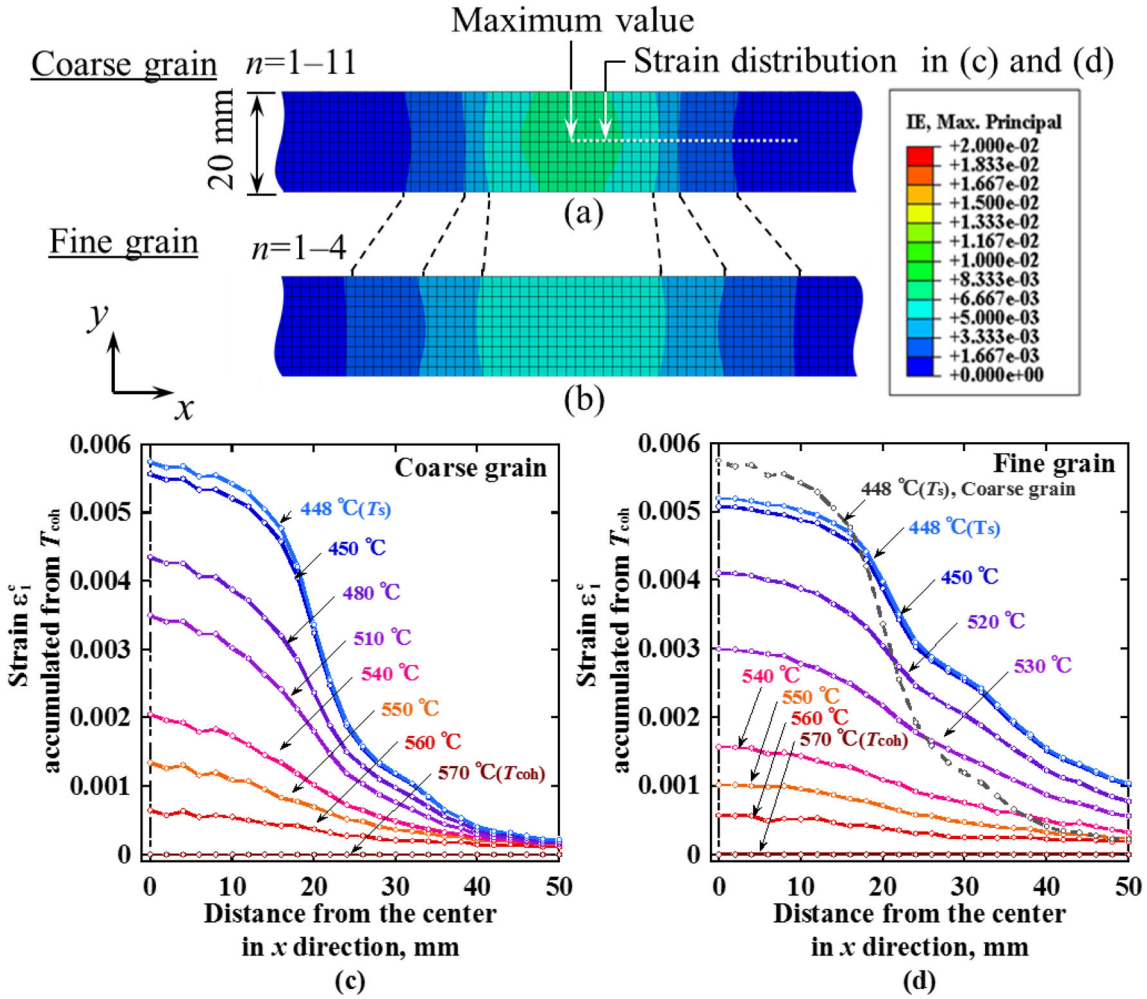


**Fig. 9** Both contour plot and distribution of the maximum strain of the creep component: coarse grain (**a**, **c**) and fine grain (**b**, **d**)

As described in Chapter 3, except for the two creep parameters, the same analytical condition was used for the two alloys. Therefore, the factor to determine the strain distribution should be in the two creep parameters. In the hot deformation of alloy in the solid state, Prasad and Seshacharyulu [39] and Narayana et al. [40] reported in their reviews that the higher value for the coefficient $m(=d\log\sigma/d\log\dot{\varepsilon} = 1/n)$ inhibits the flow localization and the flow stability. On the other hand, the semi-solid state of alloy is essentially not a continuum but the two phase material consists of solid grains and liquid film. However, the analytical result demonstrated in this study shows that higher value of the coefficient $m$ during the solidification, which is one of the two creep parameters, should be critical to more homogeneous strain distribution by the grain refinement. A theoretical approach should be a subject of future investigation to explain the relation between the strain rate sensitivity and the strain distribution in the semi-solid state of alloy with considering the microstructure change such as the formation of liquid channel reported by Sheikh Ansari and Aghaie-Khafri [41] and the grain boundary sliding reported by Takai et al. [19].

#### 4.3.2 Specimen with no shrinkage

Figure 9 shows the effect of the grain refinement on the strain distribution in the analytical model of the specimen with no external shrinkage. The maximum values of the strain for the two alloys are smaller compared to those with the external shrinkage. However, the grain refinement makes the strain distribution more uniform and reduces the maximum value of the strain as well as the result using the model with the external shrinkage. The result demonstrates that, in DC casting billets where hot tearing generally occurs inside the ingot rather than at the surface [4], the analysis using the grain size–dependent two creep parameters have the potential for considering the grain size–effect in the quantitative prediction of hot tearing tendency.

## 5 Conclusion

This study examined how the macroscopic strain during the solidification of Al–Mg alloy contributes to the reduction of

hot tearing susceptibility by the grain refinement. In the thermal stress analysis, the mechanical behavior of the alloy during the solidification was described using an elasto-creep model with the material parameters that were determined experimentally in earlier work [19, 20]. The results can be summarized as the following.

1) The grain refinement makes the calculated creep strain distribution more uniform, which in turn suppresses the maximum value of the creep strain at the final solidification part of the specimen.
2) Reduction of the maximum strain value should contribute to reducing the susceptibility to hot tearing.
3) Lower value of the strain rate sensitivity $m$ (inverse of the stress exponent $n$), which is one of the two creep parameters, is suggested to be a controlling factor for more homogeneous strain distribution during the solidification.
4) The result demonstrates that the thermal stress using the grain size–dependent two creep parameters in the semi-solid state of alloy should be an effective method to predict hot tearing tendency with considering grain size.



## References


1. Lees DCG (1946) The hot-tearing tendencies of aluminum casting alloys. J Inst Met 72:343–364
2. Lin S, Aliravci C, Pekguleryuz MO (2007) Hot-tear susceptibility of aluminum wrought alloys and the effect of grain refining. Metall Mater Trans A 38:1056–1068
3. Kimura R, Hatayama H, Shinozaki K, Murashima I, Asada J, Yoshida M (2009) Effect of grain refiner and grain size on the susceptibility of Al–Mg die casting alloy to cracking during solidification. J Mater Process Technol 209:210–219
4. Grandfield JF, Eskin DG, Bainbridge IF (2013) Direct-chill casting of light alloys. Wiley-TMS, pp:103–143
5. Pellini W (1952) Strain theory of hot tearing. Foundry 80:125–137
6. Bishop HF, Ackerlind CG, Pellini WS (1957) Investigation of metallurgical and mechanical effects in the development of hot tearing. Trans Am Foundry Soc 65:247–258
7. Campbell J (1992) Castings second edition. Butterworth-Heinemann, pp 242–258
8. Eskin DG, Suyitno, Katgerman K (2004) Mechanical properties in the semi-solid state and hot tearing of aluminium alloys. Prog Mater Sci 49:629–711
9. Magnin B, Maenner L, Katgerman L, Engler S (1996) Ductility and rheology of an Al–4.5%Cu alloy from room temperature to coherency temperature. Mater Sci Forum 222:1209–1214
10. Nagaumi H, Umeda T (2002) Prediction of internal cracking in a direct-chill cast, high strength, Al–Mg–Si alloy. J Light Met 2:161–167
11. M'Hamdi M, Benum S, Mortensen D, Fjær HG, Drezet J-M (2003) The importance of viscoplastic strain rate in the formation of center cracks during the start-up phase of direct-chill cast aluminum extrusion ingots. Metall Mater Trans A 34:1941–1952
12. Suyitno KWH, Katgerman L (2004) Finite element method simulation of mushy zone behavior during direct-chill casting of an Al–4.5 pct Cu alloy. Metall Mater Trans A 35:2918–2926
13. Pokorny M, Monroe C, Beckermann C, Bichler L, Ravindran C (2008) Prediction of hot tear formation in a magnesium alloy permanent mold casting. Int J Met 2:41–53
14. Shi Z, Dong J, Zhang M, Zheng L (2014) Hot tearing susceptibility analysis and prediction of K418 superalloy for auto turbocharger turbine wheel. Trans Nonferrous Metals Soc China 24:2737–2751
15. Prokhorov NN (1962) Resistance to hot tearing of cast metals during solidification Russian Casting Production 2:172–175
16. Phillion AB, Cockcroft SL, Lee PD (2009) Predicting the constitutive behavior of semi-solids via a direct finite element simulation: application to AA5182. Model Simul Mater Sci Eng 17:055011
17. Jamaly N, Phillion AB, Drezet J-M (2013) Stress–strain predictions of semisolid Al–Mg–Mn alloys during direct chill casting: effects of microstructure and process variables. Metall Mater Trans B Process Metall Mater Process Sci 44:1287–1295
18. Phillion AB, Cockcroft SL, Lee PD (2008) A three-phase simulation of the effect of microstructural features on semi-solid tensile deformation. Acta Mater 56:4328–4338
19. Takai R, Matsushita A, Yanagida S, Nakamura K, Yoshida M (2015) Development of an elasto-viscoplastic constitutive equation for an Al–Mg alloy undergoing a tensile test during partial solidification. Mater Trans 56:1233–1241
20. Takai R, Kimura S, Kashiuchi R, Kotaki H, Yoshida M (2016) Grain refinement effects on the strain rate sensitivity and grain boundary sliding in partially solidified Al–5 wt.%Mg alloy. Mater Sci Eng A 667:417–425
21. Takai R, Tsunoda T, Kawada Y, Hirohara R, Okane T, Yoshida M (2018) Effect of temperature field and mechanical properties of casting on prediction of hot tearing tendency using FEM thermal stress analysis. Mater Trans 59:1333–1340
22. Stangeland A, Mo A, M'Hamdi M, Viano D, Davidson C (2006) Thermal strain in the mushy zone related to hot tearing. Metall Mater Trans A 37:705–714
23. Pokorny MG, Monroe CA, Beckermann C, Zhen Z, Hort N (2010) Simulation of stresses during casting of binary Mg-Al alloys. Metall Mater Trans A 41:3196–3207
24. Giraud E, Suery M, Coret M (2010) Mechanical behavior of AA6061 aluminum in the semisolid state obtained by partial melting and partial solidification. Metall Mater Trans A 41:2257–2268
25. Hirohara R, Kawada K, Takai R, Otaki M, Okane T, Yoshida M (2017) Prediction and experimental validation of cooling rate dependence of viscoplastic properties in a partially solidified state of Al–5mass%Mg alloy. Mater Trans 58:1299–1307
26. Singer ARE, Cottrell SA (1947) Properties of the aluminum–silicon alloys at temperatures in the region of the solidus. J Inst Met 73:33–54
27. Dahle AK, Arnberg L (1997) Development of strength in solidifying aluminium alloys. Acta Mater 45:547–559
28. Metz SA, Flemings MC (1970) A fundamental study of hot tearing. AFS Trans 78:453–460
29. Kubota M, Kitaoka S (1973) Solidification behavior and hot tearing tendency of aluminum casting alloys. AFS Trans 81:424–427
30. Alankar A, Wells MA (2010) Constitutive behavior of as-cast aluminum alloys AA3104, AA5182 and AA6111 at below solidus temperatures. Mater Sci Eng A 527:7812–7820
31. Odqvist FKG (1974) Mathematical theory of creep and creep rupture second edition. Clarendon Press, pp. 22
32. Norton FH (1929) The creep of steel at high temperatures. McGraw-Hill Book Company, pp. 67
33. Bailey RW (1935) The utilization of creep test data in engineering design. Proc Inst Mech eng 131:131–349

34. Eskin DG, Suyitno MJF, Katgerman L (2004) Contraction of aluminum alloys during and after solidification. Metall Mater Trans A 35:1325–1335
35. Stangeland A, Mo A, Nielsen Ø, Eskin D, M'Hamdi M (2004) Development of thermal strain in the coherent mushy zone during solidification of aluminum alloys. Metall Mater Trans A 35: 2903–2915
36. Drezet J-M, Eggeler G (1994) High apparent creep activation energies in mushy zone microstructures. Scripta Metall Mater 31:757–762
37. Hao H, Maijer DM, Wells MA, Phillion A, Cockcroft SL (2010) Modeling the stress-strain behavior and hot tearing during direct chill casting of an AZ31 magnesium billet. Metall Mater Trans A 41:2067–2077
38. D'Elia F, Ravindran C, Sediako D (2015) Interplay among solidification, microstructure, residual strain and hot tearing in B206 aluminum alloy. Mater Sci Eng A 624:169–180
39. Prasad YVRK, Seshacharyulu T (1998) Modelling of hot deformation for microstructural control. Inter Mater Rev 43:243–258
40. Narayana Murty SVS, Nageswara Rao B, Kashyap BP (2000) Instability criteria for hot deformation of materials. Inter Mater Rev 45:15–26
41. Sheikh Ansari MH, Aghaie-Khafri M (2018) Predicting flow localization in semi-solid deformation. Inter J Mater Form 11:165–173